

1 **RAPPID: Towards Generalisable Protein Interaction Prediction with AWD-LSTM Twin Networks**

2

3

4

5 Joseph Szymborski^{1,2} and Amin Emad^{1,2,3,*}

¹ Department of Electrical and Computer Engineering, McGill University, Montréal, QC, Canada

² Mila, Quebec AI Institute, Montréal, QC, Canada

³ The Rosalind and Morris Goodman Cancer Institute, Montréal, QC, Canada

6 * Corresponding Author:

7 Amin Emad

8 755 McConnell Engineering Building

9 3480 University Street

10 Montréal, QC, Canada, H3A 0E9

11 Email: amin.emad@mcgill.ca

12 **ABSTRACT**

13 **Motivation:** Computational methods for the prediction of protein-protein interactions, while
14 important tools for researchers, are plagued by challenges in generalising to unseen proteins.
15 Datasets used for modelling protein-protein predictions are particularly predisposed to
16 information leakage and sampling biases.

17 **Results:** In this study, we introduce RAPPID, a method for the Regularised Automatic
18 Prediction of Protein-Protein Interactions using Deep Learning. RAPPID is a twin AWD-
19 LSTM network which employs multiple regularisation methods during training time to learn
20 generalised weights. Testing on stringent interaction datasets composed of proteins not seen
21 during training, RAPPID outperforms state-of-the-art methods. Further experiments show that
22 RAPPID's performance holds regardless of the particular proteins in the testing set and its
23 performance is higher for biologically supported edges. This study serves to demonstrate that
24 appropriate regularisation is an important component of overcoming the challenges of creating
25 models for protein-protein interaction prediction that generalise to unseen proteins. Additionally,
26 as part of this study, we provide datasets corresponding to several data splits of various
27 strictness, in order to facilitate assessment of PPI reconstruction methods by others in the future.

28 **Availability and Implementation:** Code and datasets are freely available at
29 <https://github.com/jszym/rappid>.

30 **Contact:** amin.emad@mcgill.ca

31 **Supplementary Information:** Online-only supplementary data is available at the journal's
32 website.

33

34 INTRODUCTION

35 Interactions of proteins with other proteins and their surroundings are fundamental to the internal
36 machinery of a cell. These interactions are of particular interest, as it is essential for a bevy of
37 diverse cellular functions: from organising cell structure to generating metabolic energy (Huttlin
38 *et al.*, 2017). These interactions are typically validated with a high degree of confidence by the
39 many biological assays commonly employed today, each with their own specific advantages and
40 challenges (Snider *et al.*, 2015). Assays for validating protein interactions range from the
41 venerable yeast two hybrid (Y2H) (Vidal and Fields, 2014) which researchers have relied on for
42 the past decades, to more recent Biotin-related techniques such as BioID-MS (Roux *et al.*, 2012).
43 A characteristic of all these assays, however, is that they are costly in terms of time, labour, and
44 materials. A further complication of protein-protein interaction studies are the multiple sources
45 of biases that plague small and large datasets alike. The choice of proteins to include in a study
46 poses a particular threat of so-called “bait bias” in smaller datasets, while large datasets suffer
47 from biases in the discovered protein interactions (“prey bias”) as well as the exacerbation of
48 laboratory biases when included in aggregated datasets (Gillis *et al.*, 2014). Entire classes of
49 proteins, such as membrane proteins, which are sometimes difficult to experimentally validate
50 are often under-represented in these interaction studies as well.

51

52 Computational approaches to predict protein-protein interactions (PPIs) are therefore useful to
53 help towards reducing the number of costly experiments researchers are required to perform.
54 Researchers have deployed many diverse approaches to solve the task of protein sequence-based
55 interaction prediction. Most sequence-based methods rely on the understanding that co-evolution
56 and co-expression of proteins are both tied to protein interaction and sequence similarity (Cong

57 *et al.*, 2019; Jansen, 2003). Some methods rely on substitution matrices for sequence alignment
58 such as BLOSUM or PAM in combination with machine learning methods to predict interactions
59 (Henikoff and Henikoff, 1992; Ding *et al.*, 2016). Other methods utilise Support Vector
60 Machines (SVMs) with kernels specifically designed for use with protein sequences (Ben-Hur
61 and Noble, 2005). Other statistical methods including naïve bayes (NB) and *k*-nearest neighbors
62 (kNN) have been used to predict protein interactions from protein sequences (Browne *et al.*,
63 2007). Some of the most successful PPI prediction methods belong to the family of methods that
64 rely on novel substring search algorithms (Li and Ilie, 2017; Dick *et al.*, 2020), operating
65 similarly to sequence search tools like BLAST (Altschul *et al.*, 1990). Deep learning models
66 have also been designed for predicting protein interactions (Chen *et al.*, 2019). These deep
67 approaches commonly either learn wide networks or share weights in a twin design; the latter
68 being shown to be both more efficient and effective (Richoux *et al.*, 2019).

69

70 Such methods, however, face many challenges due to the nature of the data on which they train.
71 Arguably the most pervasive of which is the ability of models to generalise and predict the
72 interactions of proteins previously unseen by the prediction method. To ensure such
73 generalisability, careful cross-validation techniques must be used to avoid data leakage. While
74 the necessity of appropriate cross-validation techniques is not unique to this area of research, the
75 application of these networks (e.g., PPIs, transcriptional regulatory networks) to obtain
76 biological insights makes it particularly important to address this challenge in the task of
77 biological network reconstruction (Park and Marcotte, 2012; Tabe-Bordbar *et al.*, 2018).

78

79 For PPI reconstruction, developing generalizable models prove particularly difficult. The nature
80 of PPI networks makes it easy to create datasets with testing/training splits which leak
81 information, resulting in inflated performance metrics that cannot properly assess the
82 generalisability of these methods. In particular, simply splitting interaction datasets into training
83 and testing sets using random selection of edges results in the construction of testing datasets that
84 are almost entirely comprised of interactions between proteins found in the training set. Indeed,
85 Park and Marcotte in 2012 found that all the PPI prediction models they surveyed were tested on
86 such naïvely constructed datasets (Park and Marcotte, 2012). The surveyed models, which had
87 optimised their performance on these naïve datasets, that suffered from a large degree of
88 information leakage, were also found to incur precipitous falls in their prediction metrics when
89 tested on datasets where no proteins in the testing set occurred in the training dataset.

90
91 When faced with obstacles in the construction of generalisable models, strategic and targeted
92 applications of regularisation at training time can significantly improve results. This is
93 particularly relevant in the context of deep learning methods which pay for their expressiveness
94 by learning an outsized number of parameters. Among the most common regularisation
95 techniques used in the deep learning context is "dropout" (Srivastava *et al.*, 2014). Applying
96 dropout to a layer consists of randomly zeroing the activations of the previous network with
97 some probability p . However, choice of regularisation techniques must be selected with care and
98 in accordance with the architecture. For example, applying dropout directly to the hidden state of
99 Recurrent Neural Networks (RNNs) (Lipton *et al.*, 2015), an architecture which lends itself
100 naturally to sequential inputs such as amino acid chains, impairs its ability to retain its memory
101 of previous inputs (Zaremba *et al.*, 2015).

102 Applying regularisation to RNNs requires additional considerations. Recent work by Merity *et*
103 *al.* has demonstrated that randomly zeroing the weights of RNNs (“dropconnect”) (Wan *et al.*,
104 2013) rather than their hidden state activation (“dropout”) effectively reduces testing error
105 (Merity *et al.*, 2017). Merity *et al.* describe applying dropout to the embedding layer as well as
106 using an averaged optimiser (NT-ASGD) as part of a series of regularisation techniques dubbed
107 Averaged Weight-Dropped Long Short-Term memory (AWD-LSTM). The regularisation
108 techniques used by AWD-LSTM models are specifically selected for their suitability in the
109 context of training RNNs.

110

111 To meet the generalisation challenges posed by PPI prediction tasks, we developed a method
112 called the Regularised Automatic Prediction of Protein-Protein Interactions using Deep
113 Learning, or RAPPID. RAPPID addresses the challenges in creating generalised models for
114 PPI prediction by adopting (with modification) the AWD-LSTM, a regularised recurrent neural
115 network training routine (Merity *et al.*, 2017). In this study, we showed that RAPPID
116 outperforms state-of-the-art PPI prediction methods on strict validation datasets constructed in
117 accordance with guidelines set out by Park & Marcotte (Park and Marcotte, 2012). Additionally,
118 we performed various analyses and applied RAPPID to different use-cases to show-case the
119 effect of different components of its architecture and training on its performance and its
120 applicability to different real-world scenarios.

121

122 It is worth mentioning that in addition to RAPPID’s code, we have made various pre-processed
123 datasets freely available in the hope that they facilitate the evaluation of protein interaction

124 prediction methods on datasets that both mitigate information leakage and are appropriately large
125 for deep learning applications.

126

127

128 **METHODS**

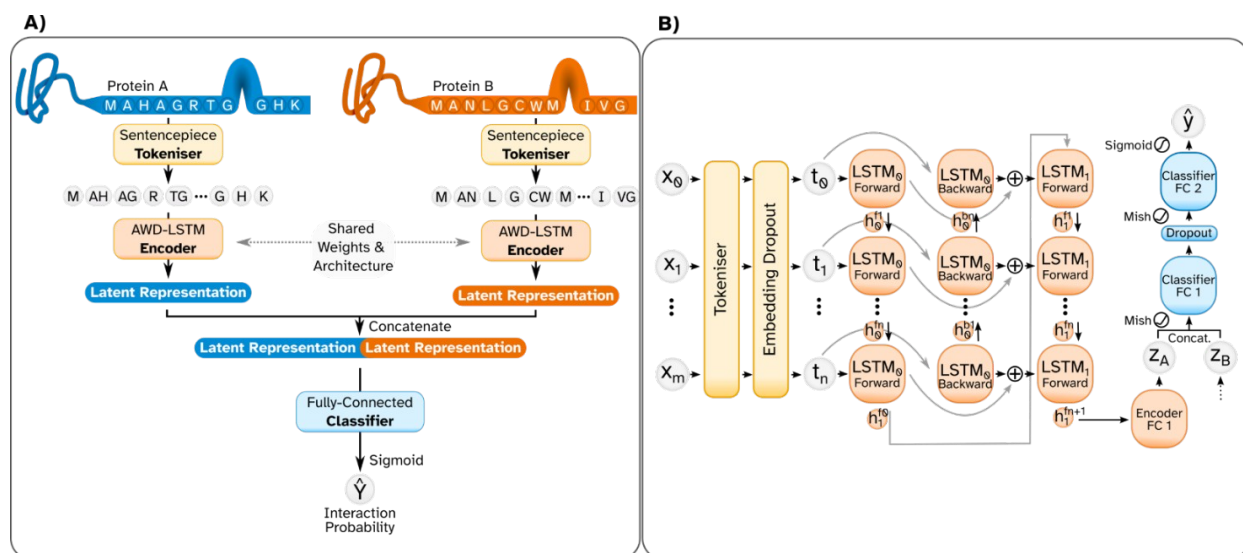
129 **PPI prediction using AWD-LSTM Twin Networks**

130 RAPPID is first trained by considering pairs of amino acid sequences of proteins along with a
131 label indicating whether they do or do not interact. The amino acid sequences are first tokenised
132 using the Sentencepiece algorithm (Kudo and Richardson, 2018), which allows for better
133 recognition of common groupings of amino acid residues that make up the secondary structure
134 and motifs of proteins. Fixed-length latent vector representations of the token sequences of both
135 proteins are then computed by twin neural networks (Bromley *et al.*, 1993), forming the encoder
136 of RAPPID's pipeline. These twin networks have shared architectures and weights and are
137 trained jointly. An overview of the pipeline is provided in Figure 1.

138

139 Each twin network consists of a two-layer bidirectional AWD-LSTM network (Merity *et al.*,
140 2017), which takes a tokenised amino acid sequence as its input and generates a fixed-length
141 latent vector representation as its output. AWD-LSTMs are architecturally identical to the
142 LSTMs (Hochreiter and Schmidhuber, 1997), however at inference time, several regularisation
143 techniques are employed while training to promote learning generalised weights. Among these
144 regularisation techniques are an averaged optimizer and dropout applied to embeddings and
145 LSTM weights (Athiwaratkun *et al.*, 2019; Wan *et al.*, 2013). Using an AWD-LSTM encoder

146 enables RAPPID to leverage the strong inductive biases of LSTMs, while ensuring that the
 147 learned weights are generalised.



148
 149 **Figure 1: Overview of the RAPPID pipeline and architecture.** (A) The pipeline of the
 150 RAPPID begins with two protein sequences. Each sequence is first tokenised by the
 151 Sentencepiece tokeniser (yellow). Each sequence of tokens is then inputted separately into an
 152 AWD-LSTM encoder layer which results in a latent representation for each protein. The latent
 153 representations of each protein are inputted into a fully-connected classifier layer. The classifier
 154 layer outputs the predicted probability of the two proteins interacting. (B) Taking a closer look at
 155 the architecture of the RAPPID, individual residues x_0 to x_m for a protein comprised of m
 156 residues are tokenized into n tokens t_0, t_1, \dots, t_n . The embedding dropout layer randomly assigns
 157 random tokens from the total vocabulary to zero. The encoder layer is comprised of a multi-layer
 158 bidirectional LSTM whose last hidden state is fed to a fully connected layer before outputting a
 159 latent representation z_A . z_A is then concatenated with the latent representation of a second protein
 160 (z_b) before being inputted into the two-layer fully-connected classifier. The output of the
 161 classifier is activated by the sigmoid function to produce a probability of interaction.

162
 163 The final hidden state of the AWD-LSTM is passed to a single fully-connected layer whose
 164 output, once activated by the Mish function (Misra, 2020), is the latent representation of the
 165 amino acid sequences. The latent representations of both proteins are then concatenated and
 166 provided as inputs to the classifier network which generates an interaction probability for each
 167 protein pair. The classifier network is a two-layer fully-connected network that outputs a single

168 logit whose sigmoid activation serves as the probability of the two proteins interacting. The
169 activated logit is then used to calculate the mean binary cross-entropy loss. Relegating the
170 pairwise comparison of proteins to the shallower classifier network allows RAPPID to infer
171 protein interactions in an efficient manner. Figure 1 provides an overview of RAPPID’s
172 pipeline.

173

174

175 **Sequence Segmentation and Tokenisation**

176 As mentioned earlier, RAPPID utilises the Sentencepiece algorithm (Kudo and Richardson,
177 2018) to tokenize amino acid sequences. While words form the basis of many natural languages
178 and may break up sentences and phrases into discrete units, no such higher-order segmentation is
179 as immediately apparent in amino acids. Motifs and protein domains possess many analogous
180 qualities to words in natural languages; they appear repeatedly in amino acid sequences and their
181 combination and relative position in these sequences play important roles in the protein structure
182 and function (Anfinsen, 1973).

183

184 Much like words, however, motifs and protein domains present an “out-of-vocabulary” problem,
185 where unseen examples are difficult to handle. Attempts to solve this problem in natural
186 language processing tasks has resulted in “subword” segmentation algorithms, particularly in
187 difficult-to-segment languages such as Japanese which do not separate words by spaces (Schuster
188 and Nakajima, 2012). Here, we employ the Sentencepiece algorithm (Kudo and Richardson,
189 2018) to sample tokens from “subword” vocabularies generated by the Unigram algorithm
190 (Kudo, 2018). The unigram and sentencepiece algorithms construct vocabularies of arbitrary size

191 by modelling the probabilities of subwords and provides a principled manner for sampling from
192 this distribution to reconstruct sequences. The multi-residue tokens that comprise the vocabulary
193 subdivide low-entropy areas and reduce the overall length of the sequences encoded.

194

195

196 **Generalising Protein Sequence Encoding with AWD-LSTM**

197 The task of protein-protein interaction prediction on unseen proteins is a difficult problem prone
198 to overfitting, as demonstrated by the poor testing performance of various methods on unseen
199 proteins (Park and Marcotte, 2012). For this reason, a training and optimisation methodology that
200 allows efficient regularisation is desirable. AWD-LSTM was recently devised to enable efficient
201 training of generalisable recurrent neural networks (RNNs) (Merity *et al.*, 2017). This approach
202 deploys several regularisation techniques during training to achieve this goal. RAPPID adopts,
203 with modification, the training methodology of AWD-LSTM.

204

205 RAPPID utilises Embedding Dropout, DropConnect (Wan *et al.*, 2013), and Weight Decay
206 (Loshchilov and Hutter, 2019) on the LSTM weights, as described by AWD-LSTM, in the
207 encoder during training. Both AWD-LSTM and RAPPID optimise over average weights,
208 however the optimisers are quite different. AWD-LSTM makes use of the non-monotonically
209 triggered averaged stochastic gradient descent (NT-SGD) optimiser which switches between
210 stochastic gradient descent (SGD) and the averaged variant (ASGD). RAPPID uses the recent
211 Stochastic Weight Averaging (SWA) strategy in combination with the Ranger21 optimiser
212 (Athiwaratkun *et al.*, 2019; Wright and Demeure, 2021).

213

214 SWA has been shown to promote generalisable models in part by overcoming the challenges of
215 finding best solutions within flat loss basins (Izmailov *et al.*, 2019). Ranger21 is an optimiser that
216 applies the “Lookahead mechanism” (Zhang *et al.*, 2019) to the AdamW optimiser (Loshchilov
217 and Hutter, 2019) and includes several optimisation techniques (Wright and Demeure, 2021).
218 These techniques, which include gradient centralisation and adaptive gradient clipping, enable us
219 to further improve our ability to learn generalised weights and smooth training trajectories
220 (Brock *et al.*, 2021; Yong *et al.*, 2020). Finally, since RAPPID does not rely on the timestep
221 outputs of the LSTM network, the Temporal Regularisation (TAR) described by AWD-LSTM is
222 not applicable.

223

224

225 **Details of RAPPID’s architecture and hyperparameter tuning**

226 The dimensionality of the AWD-LSTM hidden state is made equal to the dimensionality of the
227 embeddings (*i.e.*, 64). The output of the fully-connected layer is of equal dimensionality to that
228 of the AWD-LSTM hidden state and is activated by the Mish activation function (Misra, 2020).
229 The output of the first fully-connected layer is half the size of the embedding dimension,
230 activated by the Mish function, and regularised by a dropout layer (Srivastava *et al.*, 2014).
231 RAPPID trains on a vocabulary of 250 tokens that is generated by the Sentencepiece algorithm.
232 New vocabularies are generated for each dataset before training.

233

234 The number of LSTM layers, L2 coefficient, and various dropout rates are defined as hyper-
235 parameters that require tuning between different datasets. Hyper-parameters were selected by
236 cross-validation. The range of considered hyperparameters and their selected values are provided

237 in the Supplementary Tables S1-S2 (in Supplementary File 1). The chosen hyper-parameter
238 ranges are a compromise between common, reasonable values and maintaining a manageable
239 hyper-parameter space which can be explored practically.

240

241

242 **Protein Interaction Datasets**

243 We obtained protein-protein interactions (PPIs) and protein sequences from version 11 of the
244 Search Tool for the Retrieval of Interacting Genes/Proteins (STRING) database (Szklarczyk *et*
245 *al.*, 2019), from the official STRING website. Edges were downloaded from [https://stringdb-](https://stringdb-static.org/download/protein.links.detailed.v11.0.txt.gz)
246 [static.org/download/protein.links.detailed.v11.0.txt.gz](https://stringdb-static.org/download/protein.links.detailed.v11.0.txt.gz) and sequences were downloaded from
247 <https://stringdb-static.org/download/protein.sequences.v11.0.fa.gz>. In this dataset, the association
248 between any two proteins is assigned a confidence score depending on the source of the
249 information (called a “channel”). In our analyses, only associations with a combined STRING-
250 score above 95% (equivalent to a score above 950, obtained from combining different channels)
251 were considered as positive edges. We also retained the channel-specific scores for further
252 analysis.

253

254 To obtain an estimate of the false-positive rate of the confidence score-filtered STRING dataset,
255 we leveraged the curated and experimentally validated non-interacting protein pairs from the
256 Negatome dataset (Blohm *et al.*, 2014). By comparing the set of proteins that are in both
257 STRING and Negatome, and evaluating the number of negative edges in Negatome that were
258 considered a positive edge in this intersection, we estimated the false-positive rate of our

259 STRING dataset to be 4.01%. This false-positive rate is within the expected 5% upper-bound
260 given by our 95% confidence threshold.

261

262 PPI graphs are understood to be scale-free in the general case. This property of PPI graphs can
263 make them challenging datasets upon which to train a generalised model, as some proteins can
264 be over-represented. To characterise the extent to which proteins are represented in the dataset,
265 we calculated the distribution of the relative degree of proteins in the network (Supplementary
266 Figure S1A-C). The vast majority of proteins (upwards of 85%) have edges with fewer than 1%
267 of proteins within their dataset split (*i.e.*, train/validation/test). The protein with the highest
268 degree is CDC5L which has a relative degree of just over 10%, while the second highest has a
269 relative degree of 6.2% (Supplementary Figure S1D-F).

270

271

272 **Negative Examples**

273 The preparation of datasets of pairs of proteins which are known not to interact with one another
274 is a fraught process. Various methods are typically deployed to create such datasets, which are
275 integral for machine learning methods as they typically require negative examples. Ideally, only
276 negative examples are entirely composed of non-interacting protein pairs which are
277 experimentally verified and manually curated, such as the Negatome database (Blohm *et al.*,
278 2014).

279

280 Unfortunately, non-interacting pairs are difficult to experimentally validate. As a result, there are
281 far fewer *H. sapiens* negative protein pairs in such datasets such as Negatome than positive

282 protein pairs in databases such as STRING. Precisely, there are 1,191 negative *H. sapiens* pairs
283 in Negatome, and 263,130 positive pairs above a 95% confidence threshold in STRING (only
284 pairs comprised of proteins present in UniprotKB were included in this analysis). The resulting
285 class imbalance is detrimental to learning performant, generalisable models.

286

287 Synthetic negative pairs are often used to compensate for the small number of experimentally
288 verified non-interacting pairs is construction of synthetic negative pairs. A common method for
289 constructing negative pairs is to select pairs of proteins from distinct sub-cellular compartments.
290 This method has unfortunately been shown to result in biased samples according to multiple
291 measures (Ben-Hur and Noble, 2006). Selecting pairs at random from the space of pairs not
292 known to interact has proven to evade such biases, but runs the risk of capturing yet unknown
293 false-negatives. Unless otherwise noted, RAPPID utilises synthetic random pairs of proteins
294 which are not known to interact.

295

296

297 **Training, Validation and Testing Set Construction**

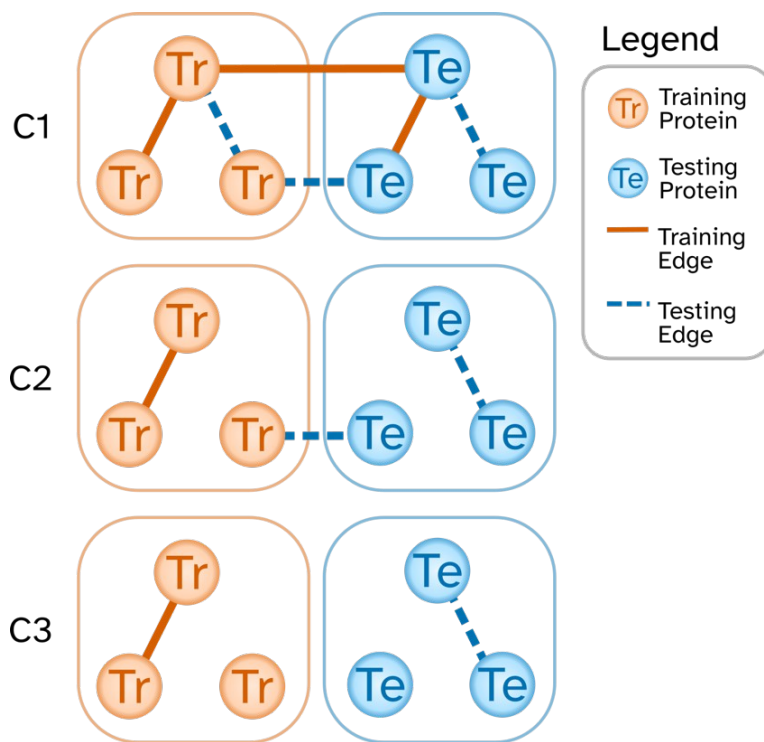
298 As identified by Park and Marcotte (Park and Marcotte, 2012), methods which consider the
299 interaction of proteins in a pairwise fashion must (and have historically failed to) take additional
300 care to avoid information leakage when constructing training and testing datasets. Following
301 their suggestion, here we use three different classes of testing and training sets to evaluate the
302 performance of RAPPID and other algorithms (Figure 2).

303

304 1) “C1” refers to the evaluation scheme in which edges (pairs of proteins) are randomly selected
305 to form the training or testing sets. Since the selection criterion is based on edges, both proteins
306 in the pair may be present in both the testing and training sets (due to the presence of other edges
307 adjacent to each protein).

308 2) “C2” refers to the evaluation scheme in which proteins are randomly selected to form the
309 training or testing sets. In this scheme, only one protein in a pair may be present in both testing
310 and training sets (but never both). This evaluation scheme mimics the scenario in which a model
311 trained on the interactome is used to predict the interaction of known proteins with a newly
312 discovered protein (that was not used to train the model).

313 3) “C3” refers to the evaluation scheme in which proteins are randomly selected to form the
314 training or testing sets. However, unlike C2, proteins which appear in the training set never
315 appear in the testing set. This is the most strict evaluation scheme.



316

317 **Figure 2: Illustration of differences in edges between C1, C2, and C3 datasets.** Differences
318 between C1, C2, and C3 datasets are most visible by first dividing the population of all proteins
319 in the dataset into training (orange, left) and testing (blue, right). In the case of the strict C3
320 dataset (bottom row), edges known at training time (orange, solid) only occur between training
321 proteins. Similarly, C3 datasets are evaluated on testing edges (blue, dotted) that only occur
322 between testing proteins. The C2 dataset has all the edges present in the C3 dataset, but also
323 includes testing edges between testing proteins and training proteins. Finally, the pervasive C1
324 datasets allows all possible training and testing edges that are not identical.

325

326 While most methods have typically reported on models validated with datasets in the C1 class,
327 they often perform much worse on similar datasets in the more conservative C2 and C3 class.
328 This is likely due to the information leakage between training and testing sets present in the C1
329 class and, to a lesser extent, in the C2 class. In our evaluations, we report the performance of
330 different methods using all three evaluation schemes above, but we are most interested in the
331 results of C3 due to a lack of information leakage.

332

333 In the C-type datasets we've created, there are approximately 9.3 thousand proteins. The number
334 of edges in the datasets range from just over 263 thousand edges in the C1 dataset to just under
335 174 thousand edges in the C3 dataset. Full dataset statistics are presented in Supplementary
336 Table S3. These C-type datasets are made freely available to the public, with instructions on how
337 to download them at <https://github.com/jszym/rappid/tree/main/data>. We've made these
338 datasets available in the hope that it facilitates the evaluation of protein interaction prediction
339 methods on datasets that both mitigate information leakage and are appropriately large for deep
340 learning applications. The adoption of C-type datasets for training and evaluation of PPI
341 prediction methods is important for accurate and representative benchmarking.

342

343

344 **Implementation**

345 RAPPID was implemented in the Python computer language using the PyTorch and PyTorch
346 Lightning deep learning framework (Paszke *et al.*, 2019; Falcon *et al.*, 2020). Embedding
347 Dropout and DropConnect implementation were obtained from the AWD-LSTM code base
348 (Merity *et al.*, 2017). The source code for RAPPID can be found by visiting
349 <https://github.com/jszym/rappid>. RAPPID was trained at a rate of approximately 2.7 training
350 steps per second at a batch size of 80 protein pairs on an NVIDIA RTX 2080 GPU and 32 CPU
351 cores clocked at 2.2 GHz. The C3 model takes approximately 2.4 hours to train, while C1 and C2
352 take approximately 7.8 hours.

353

354

355

356 **Protein Similarity Experiments**

357 In the analysis of the sequence similarity between testing and training proteins, “Percent
358 Identity” was measured between proteins using NCBI’s PSI-BLAST tool running locally as part
359 of version 2.12.0 of NCBI’s BLAST+ software suite (Altschul *et al.*, 1997). In addition to the
360 Percent Identity, for two proteins to be considered similar, an E-value cut-off of at most 5 and an
361 alignment length of more than 30% of the query sequence were considered necessary. The 64-bit
362 Linux binaries of the BLAST+ suite were obtained from the link
363 <ftp.ncbi.nlm.nih.gov/blast/executables/blast+/2.12.0/>.

364

365

366 **Results**

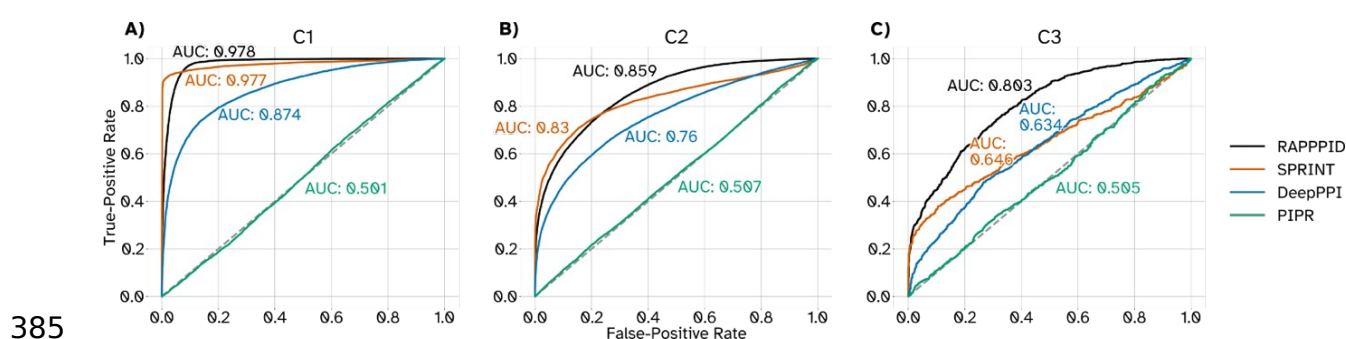
367 **Performance evaluation of RAPPID and other algorithms**

368 To establish the ability of RAPPID to correctly predict protein-protein interactions within the
369 current landscape of PPI prediction methods, we compared it against three recent methods
370 (Figure 3). The first of these is the Scoring Protein INteractions (SPRINT) method, which
371 belongs to the family of methods that predict interactions according to measures of sequence
372 similarity (Li and Ilie, 2017). SPRINT was shown to outperform support-vector machine
373 (SVM), random-forest (RF), and sequence similarity-based methods across C1, C2, and C3-like
374 datasets.

375

376 The two other methods, PIPR and DeepPPI, are deep learning methods that similar to RAPPID
377 utilize twin networks (Chen *et al.*, 2019; Richoux *et al.*, 2019). PIPR uses a residual recurrent
378 convolutional neural network (RCNN) for its encoder with the goal of more effectively

379 summarising both local and global features. We compared RAPPPID against the best performing
380 iteration of DeepPPI, whose encoder comprises of a convolutional neural network feature
381 extractor followed by an LSTM network. All three methods required retraining, as the available
382 weights of these models belong to diverse datasets, all of which are either not C2 or C3 type, or
383 (in the case of SPRINT) are insufficiently large for training a generalisable deep learning model.
384



386 **Figure 3. Receiver-Operator curves across methods and datasets.** The receiver-operator
387 curves (ROCs) for all four methods tested across C1 (A), C2 (B), and C3 (C) datasets.

388

389 Across C1, C2, and C3 testing datasets, RAPPPID achieved higher area under the receiver-
390 operator curve (AUROC) than all other methods tested (Table 1). The margin between RAPPPID
391 and the second highest performing method (SPRINT in all cases) was highest when performed
392 on the stricter C3 dataset, resulting in approximately a 24.3% improvement. The improvement
393 obtained by RAPPPID compared to SPRINT was lower on the C2 dataset (approximately 3.4%),
394 and finally nearly equivalent on the least strict C1 dataset.

395

396 With regards to the area under the precision-recall curve (AUPR), this trend across dataset types
397 persisted. RAPPPID's AUPR was higher than all other methods for the C3 dataset, with a margin

398 to the second highest method of 0.094 (equivalent to an approximately 14.6% improvement).
399 RAPPID's AUPR score was matched by SPRINT in experiments conducted on the C2 dataset,
400 but outperformed DeepPPI and PIPR. SPRINT achieved the highest AUPR of all the methods in
401 the C1 dataset, outperforming RAPPID with a margin of 0.009 (equivalent to an approximately
402 0.9% improvement).

403 **Table 1: Comparison of PPI prediction performance on C1, C2, and C3 datasets.** The
404 testing AUROC and AUPR of four different PPI prediction methods is reported across the three
405 different dataset types described by Park & Marcotte (Park and Marcotte, 2012).

Dataset	Method	Testing AUROC	Testing AUPR
C1	RAPPID	0.978	0.974
	SPRINT	0.977	0.983
	DeepPPI	0.874	0.881
	PIPR	0.501	0.405
C2	RAPPID	0.859	0.868
	SPRINT	0.830	0.868
	DeepPPI	0.760	0.787
	PIPR	0.507	0.508
C3	RAPPID	0.803	0.810
	SPRINT	0.646	0.716
	DeepPPI	0.574	0.590
	PIPR	0.505	0.509

406
407 While we were able to replicate results of the PIPR model on the *S. cerevisiae* dataset published
408 as part of the original PIPR publication (Chen *et al.*, 2019), PIPR suffered from convergence
409 issues during training on our *H. sapiens* STRING datasets. We suspect this is due to a variety of
410 factors, with the large differences in dataset characteristics being the most likely cause. The
411 number of proteins and interactions in the *S. cerevisiae* dataset is far smaller than our STRING

412 datasets. Furthermore, the *S. cerevisiae* dataset selected pairs of proteins which occupy different
413 subcellular compartments in order to construct negative samples; an approach found to lead to
414 biased estimations of prediction accuracy (Ben-Hur and Noble, 2006).

415

416 Taken together, these results suggest that RAPPID outperforms alternative methods in the
417 majority of evaluations on C1, C2, and C3 schemes and is particularly effective in the stricter and
418 more difficult C3 evaluation.

419

420

421 **Channel-specific performance of RAPPID**

422 The STRING database, integrates and annotates protein association data from a wide range of
423 sources. The “database”, “text-mining”, “experiments”, and “coexpression” channels make-up
424 the majority of the edges in our datasets (e.g., 98.4% of all the edges in the C3 dataset).

425

426 The “database” channel is comprised of several curated databases of interactions such as KEGG
427 and Reactome (Kanehisa, 2000; Jassal *et al.*, 2019). Edges in the “text-mining” channel are the
428 result of a statistical analysis of proteins whose names and/or identifiers co-occur in publications.

429 The “experiments” channel is populated by interactions evidenced by high-throughput

430 experiments curated by members of the International Molecular Exchange (IMEx) consortium

431 (Orchard *et al.*, 2012). This includes datasets such as IntAct, DIP, the BioGRID, and many

432 others (Orchard *et al.*, 2014; Salwinski *et al.*, 2004; Oughtred *et al.*, 2020). Finally, the

433 “coexpression” channel arises from proteomic and transcriptomic assays which quantify gene-

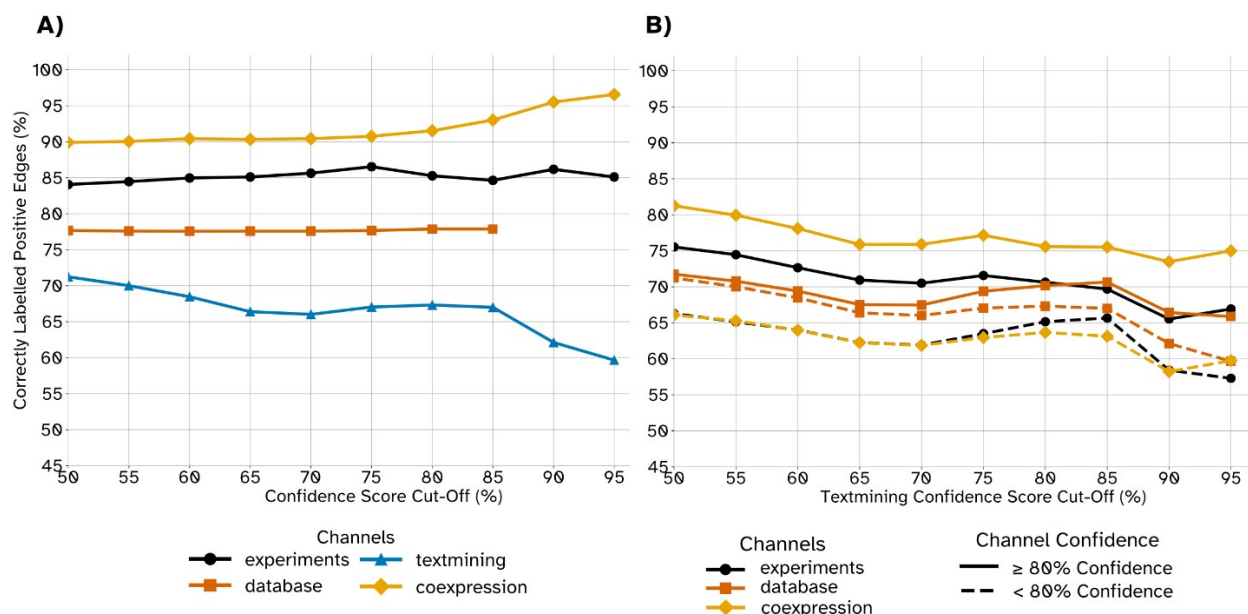
434 by-gene correlations. STRING additionally assigns calibrated confidence scores to each of the

435 edges which summarise the evidence supporting an edge. Scores are assigned to each edge by
436 channel, and finally harmonised into a final “combined confidence score” which represents the
437 evidence across all channels present in STRING.”

438

439 To better characterise the results of our protein-protein prediction tests, we sought to identify the
440 source of the testing edges RAPPID correctly and incorrectly identified. Figure 4A and
441 Supplementary Figure S2 show that RAPPID can accurately predict the testing set edges that
442 have a high confidence score in biologically supported channels of co-expression, experiments,
443 and database. However, the accuracy for the edges that have a high confidence score in the text-
444 mining channel is inferior to the other channels. Since edges that are only supported by text-
445 mining (but not by the other channels) are arguably the ones most prone to error, we expected
446 RAPPID to have an inferior performance on such edges (since the edges themselves may not be
447 reliable). To test whether the inferior performance of RAPPID in the text-mining channel in
448 Figure 4A are indeed due to such edges, for a fixed threshold k ($50 \leq k \leq 95$), we divided the
449 testing edges with a text-mining confidence score at least equal to k into two groups: a group
450 with "experiments" confidence score at least equal to 80% and a group with "experiments"
451 confidence score smaller than 80% (Figure 4B). Evaluating the testing edges in C1, C2, and C3
452 showed that for this channel, the accuracy on the former group is higher than the latter group
453 (sometimes as large as ~22% higher, Supplementary Figure S3). Repeating the analysis for co-
454 expression and database channels also confirmed this trend (Figure 4B, Supplementary Figure
455 S3). Taken together, these results suggest that the inferior performance of RAPPID on the text-
456 mining channel in Figure 4A is indeed due to the edges that are supported only by text-mining
457 and not by other biologically identified channels.

458



459

460 **Figure 4: Accuracy of positive edges across edge confidence stratified by STRING channels.**

461 (A) The percentage of correctly labelled positive edges are plotted for each major STRING
462 channel. The x-axis denotes the channel edge confidence cut-off score for each curve's respective
463 channel. (B) Here, we see a similar chart but rather than using each channel's respective score as
464 a confidence cut-off, edges are excluded according to their text-mining confidence (x-axis). The
465 solid curves include edges which have a channel confidence $\geq 80\%$ for the channel indicated by
466 the curve's colour. Dashed curves conversely include edges whose channel confidence is $< 80\%$
467 for the channel indicated by the curve's colour. In both (A) and (B) data shown reflects the C2
468 model/dataset.

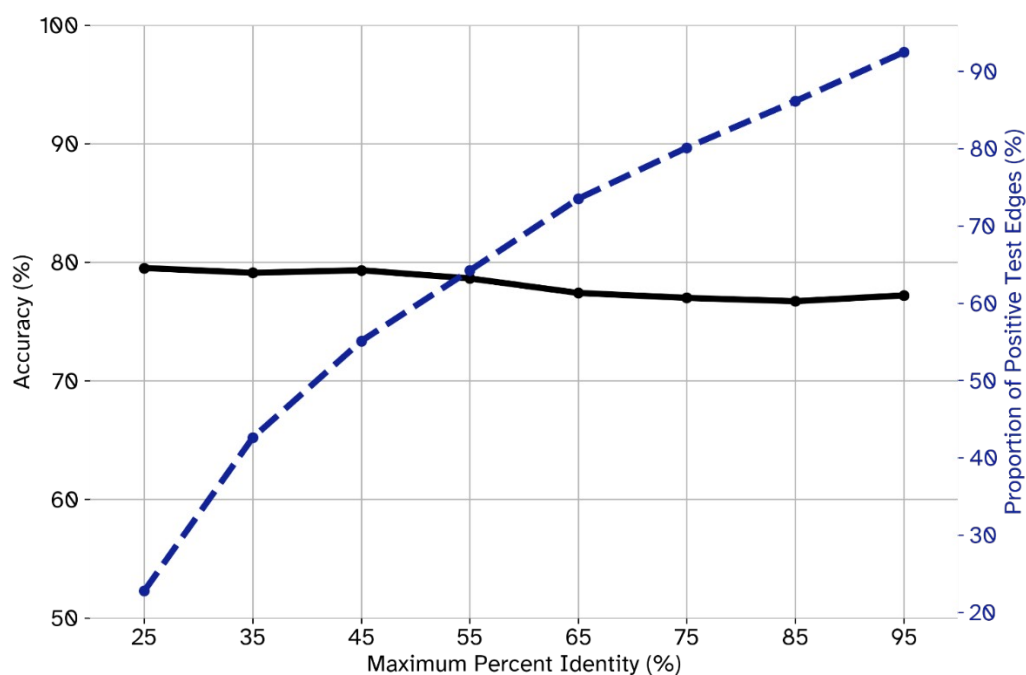
469

470

471 **Role of Protein Similarity on RAPPID's Performance**

472 The procedures for C2 and C3 datasets were devised to reduce the information leakage by
473 avoiding testing on edges which contain proteins which are known to an algorithm during its
474 training. This safeguard against information leakage, however, does not account for proteins
475 which are known by different identifiers but share near identical protein sequences. Further
476 complicating the matter, sequence similarity is a valid PPI prediction feature and is often used by

477 methods as a proxy measure of co-evolution and conserved functional domains (Cong *et al.*,
478 2019; Jansen, 2003). Indeed, this strategy is leveraged by the SPRINT algorithm against which
479 RAPPID was compared.



480 **Figure 5: Accuracy of positive edges as a function of similarity between testing and training**
481 **proteins in C2.** The similarity between testing and training proteins was measured using their
482 percent identity as computed by NCBI’s PSI-BLAST software. The highest percent identity
483 between any training protein and a testing protein in a testing edge was considered to be that
484 testing edge’s “maximum percent identity”. The percentage of accurately labelled positive edges
485 (black curve, left y-axis) is reported for edges with maximum percent identities lower than the
486 threshold reported on the x-axis. The proportion of testing edges for each threshold values is
487 reported by the dashed blue curve and the right y-axis.
488
489

490 In spite of the challenges above, we sought to determine whether the superior performance of
491 RAPPID (particularly in the strict datasets of C2 and C3) is due to sequence similarity between
492 testing and training proteins or not. For this purpose, we used PSI-BLAST algorithm (Altschul *et*
493 *al.*, 1997) to evaluate sequence similarities between each pair of testing/training proteins. Figure

494 5 shows the accuracy of RAPPID on the C2 dataset when different degrees of restriction on
495 sequence similarity are imposed. More specifically, a threshold t (x-axis in Figure 5) determined
496 the maximum allowable Percent Identity score between a testing protein and any of the training
497 proteins that were candidates to be similar to it (see Methods for details). Any testing protein that
498 did not satisfy this condition for the threshold t was excluded from the calculation of accuracy.
499 As one moves towards larger values of t , the sequence similarity constraint loosens and $t=100\%$
500 is equivalent to the complete C2 dataset. Our analysis on C2 (Figure 5) and C3 (Supplementary
501 Figure S4) revealed that RAPPID's accuracy is largely independent of the sequence similarities
502 between testing and training proteins and the performance of RAPPID does not deteriorate
503 when removing testing proteins that have a highly similar training protein.

504

505

506 **Effect of different components on RAPPID's performance**

507 To understand RAPPID's performance when trained and tested on negative examples which are
508 experimentally validated and manually curated, we created a new C3 dataset where the negative
509 examples are provided by the Negatome database of non-interacting pairs. To combat the large
510 class imbalance caused by the relatively few pairs of human proteins in Negatome (see Methods
511 for details), additional random pair negatives were supplemented until both positive and negative
512 classes had an equal number of samples. After 13 epochs, RAPPID achieved a testing AUROC
513 of 0.802 and a testing AUPR of 0.799 on C3 dataset, which is comparable to the performance of
514 RAPPID using randomly selected negative edges.

515

516 Since RAPPID utilizes random initialisation, mini-batch sampling, and token sampling, there is
517 some stochasticity present in its performance. First, we sought to test the effect of these
518 stochastic components and to ensure that the specific choice of training and test sets were not
519 responsible for the superior performance of RAPPID. For this purpose, we ran RAPPID twice
520 on three additional C3 datasets whose training, validation, and testing proteins were chosen at
521 random (a total of six times). In each of these runs, different seeds were used to assess the effect
522 of stochastic components of RAPPID (Table 2). Overall, the average testing AUROC across
523 models trained on these additional three datasets was 0.792 (± 0.007). Results from these
524 repeatability experiments illustrate that RAPPID’s strong performance on C3 datasets is not
525 tied to a specific set of testing or validation proteins, nor certain weight initialisation states.

526

527 Next, we conducted an ablation study (Table 2) using the same three C3 datasets and two runs of
528 each variant per dataset (a total of six models per variant). Each variant substitutes one
529 component of RAPPID’s regularisation, architecture or optimisation, allowing us to quantify
530 the difference in performance for which these components are responsible. In this table,
531 “RAPPID-SWA” variant removes SWA, “RAPPID+Adam” replaces Ranger21 with Adam
532 optimizer (learning rate selected by hyperparameter tuning), “RAPPID-AWD” removes the
533 AWD regularisation, and “RAPPID-SentencePiece” substitutes the SentencePiece tokens with
534 amino-acid-residue-level tokens. As can be seen in this table, the choice of optimizer has
535 negligible effect on the performance. However, SWA, AWD, and SentencePiece tokens all
536 contribute to the superior performance of RAPPID, with the tokeniser having the largest
537 contribution. One advantage that SentencePiece affords RAPPID is the regularising effect of
538 random sampling tokens. Additionally, the SentencePiece tokeniser reduces the total length of

539 sequences inputted into the tokeniser. The protein sequences on which RAPPID is trained,
540 while limited to 1,500 residues, are sufficiently large enough for gradients to vanish quiet
541 substantially; a phenomenon long known to plague RNNs when trained on long sequences
542 (Hochreiter, 1998).

543

544 **Table 3: Results from an ablation study conducted on RAPPID.** Each model is
545 trained/tested twice on three randomly generated C3 datasets. The performance metrics
546 correspond to held-out test sets.

	RAPPID (original)	RAPPID- SWA	RAPPID +Adam	RAPPID- AWD	RAPPID- SentencePiece	RAPPID +TransfLG	RAPPID +TransfSM
Test AUROC	0.792 (±0.007)	0.782 (±0.007)	0.791 (±0.025)	0.762 (±0.020)	0.749 (±0.009)	0.670 (±0.030)	0.747 (±0.026)
AUROC Diff	N/A	-1.20%	-0.100%	-3.70%	-5.37%	-15.3%	-5.68%
Test APR	0.794 (±0.009)	0.783 (±0.007)	0.792 (±0.032)	0.757 (±0.022)	0.748 (±0.011)	0.686 (±0.040)	0.758 (±0.025)
APR Diff	N/A	-1.37%	-0.273%	-4.62%	-5.85%	-13.6%	-4.61%

547

548

549 In acknowledgment of the recent prevalence and performance of attention-based methods in deep
550 learning (Vaswani *et al.*, 2017), the sixth and seventh variants replace the AWD-LSTM encoder
551 with transformers of varying sizes. “RAPPID+TransfLG” has six layers and eight heads and
552 feed-forward networks with 2048 dimensions, while “RAPPID+TransfSM” has fewer
553 parameters (two layers, two heads, and 80 dimensions). Both transformer variants have a dropout
554 rate of 20%. The number of heads and layers in RAPPID+TransfLG were chosen to closely
555 match those used in the BERT language model (Devlin *et al.*, 2019) whose architecture has been
556 previously used for predicting protein function (Elnaggar *et al.*, 2021). The number of heads and
557 layers for RAPPID+TransfSM were chosen to be representative of reasonable lower bounds for

558 those hyper-parameters. The results of these analyses (Table 2) reveal that both of these models
559 have a worse performance compared to the original RAPPID model. The superior performance
560 of the small transformer compared to the large one suggests that the large number of parameters
561 required by transformers are leading to severe overfitting in this task and are the reason behind
562 the performance deterioration

563

564

565 **Transfer Learning on Protein-Ligand Data from X-Ray Crystallography Experiments**

566 RAPPID's strong performance on C3 datasets demonstrate that it is capable of generalising to
567 predictions between proteins absent from the training set. Additionally, the ability to generalise
568 these models to make predictions on test datasets that are not representative of the training data
569 (e.g., different types of experiments or protocols are used to generate them) is also often
570 desirable, yet is often much more challenging. Transfer learning is one approach that can be used
571 to overcome the challenges imposed by differences between training and test datasets. Transfer
572 learning is the process by which a network is first trained on a large, high-quality dataset. Many
573 of these weights are then "frozen" such that they are no longer backpropagated through, while
574 the remaining "unfrozen" weights are trained on a dataset that is often smaller and/or belong to a
575 different input distribution (Yosinski *et al.*, 2014). Here, we use this approach to tackle an
576 interaction prediction task on a dataset that differs fundamentally from STRING: protein-ligand
577 interactions and sequences as determined from X-ray crystallography data.

578

579 STRING and similar PPI datasets curate interactions from a wide range of modalities and
580 provide sequences from reference proteomes. We've constructed a protein-ligand interaction task

581 by leveraging BioLiP, a semi-manually curated list of X-ray crystallography experiments
582 recorded in the Protein Data Bank (PDB) which reflect interactions between proteins and ligands
583 (Yang *et al.*, 2012; Berman, 2000). Using these datasets, we were able to extract sequences from
584 the PDB records and, after filtering out interactions with low-quality sequences, construct a
585 novel protein-ligand dataset. This dataset is available for download at
586 <https://github.com/jszym/rapppid>. The sequences extracted from PDB are measured by
587 fundamentally different modalities from those present in STRING/UniprotKB, and are often
588 truncated and incomplete as a result. Furthermore, the nature of the interactions recorded by
589 BioLiP are fundamentally different from STRING. Whereas STRING catalogues interactions
590 between large classes of proteins, the nature of X-ray crystallography biases captured
591 interactions to those with slower molecular dynamics and which do not primarily exist in
592 aliphatic environments (Carpenter *et al.*, 2008). These fundamental differences between BioLiP
593 and STRING make them ideal datasets to illustrate the ability to use transfer learning with
594 RAPPID.

595

596 We first pre-trained RAPPID on data from STRING, and then fine-tuned it on the BioLiP
597 dataset after the LSTM encoder weights were frozen, leaving only the fully-connected classifier
598 to be trained. To ensure no data leakage between the STRING and BioLiP datasets exist, protein
599 sequences in STRING determined to have more than 90% identity with those in BioLiP were
600 moved from the pre-training dataset to the fine-tuning dataset. C3-type training, validation, and
601 testing splits were constructed for both the pretraining and fine-tuning datasets for evaluation
602 purposes. Using this approach, RAPPID pre-trained on the STRING dataset and fine-tuned on a
603 portion of the BioLiP dataset achieved an AUROC of 0.909. To test our hypothesis that transfer

604 learning is indeed necessary to achieve good performance on this dataset, we also directly
605 applied the pre-trained RAPPID model (without any fine-tuning on BioLip) to the BioLip test
606 split. As expected, this resulted in almost random results (AUROC = 0.548). These results
607 highlight the difficulties of generalising a model to fundamentally different datasets and
608 emphasise the utility of transfer learning to achieve good performance using RAPPID in such
609 scenarios.

610

611

612 **RAPPID predicts interaction of HER2 with Trastuzumab and Pertuzumab**

613 Peptides and proteins have emerged as an important class of therapeutics, enabling researchers to
614 target previously “undruggable” targets (Tsomaia, 2015). Hundreds of peptide and protein
615 therapeutics have been approved by the U.S. Food and Drug Administration (Usmani *et al.*,
616 2017) with applications in treating illnesses ranging from cancer to heart disease (Sikder *et al.*,
617 2019; Chen *et al.*, 2012). Here, we sought to illustrate how one might use RAPPID to validate
618 hypothesised interactions between target proteins and candidate therapeutic proteins and peptides
619 through two examples: Trastuzumab and Pertuzumab.

620

621 Trastuzumab and Pertuzumab are two recombinant humanised monoclonal antibodies which are
622 used in combination in the treatment of metastatic breast cancers which belong to the HER2-
623 positive subtype (Boekhout *et al.*, 2011; Malenfant *et al.*, 2014). Both Trastuzumab and
624 Pertuzumab target distinct domains of the human epidermal growth factor receptor 2 (HER2).
625 We applied RAPPID, trained on our *H. sapiens* STRING C2 dataset (which is more appropriate
626 for this application), to the sequences of the Trastuzumab and Pertuzumab antibody chains.

627 RAPPID predicted that HER2 interacts with Trastuzumab and Pertuzumab with 86.20% and
628 95.11% probability, respectively. This suggests that RAPPID may be utilized as part of an
629 interaction-based low-cost filtering or early validation step in the development of therapeutic
630 proteins and peptides.

631

632

633 **Discussion and Conclusion**

634 This study introduced RAPPID, a deep learning method that addresses the challenges of
635 creating generalisable PPI prediction models posed by inherent characteristics of PPI datasets.
636 By adopting a modified AWD-LSTM training routine, RAPPID was able to surpass state-of-
637 the-art models under testing conditions that carefully controlled for information leakage and
638 other sources of prediction accuracy inflation. Further experiments were conducted to confirm
639 the results were independent of the specific proteins present in the training and testing splits.
640 RAPPID's ability to PPIs in the STRING database was shown to increase with strong biological
641 evidence for the interaction. This relationship between PPI evidence and RAPPID predictive
642 ability illustrates that RAPPID accurately reflects our confidence in interactions, and testing
643 performance is not disproportionately inflated by spurious, low-confidence interactions.
644 Moreover, assessment of the sequence similarity between testing and training proteins revealed
645 that the superior performance of RAPPID is not due to the presence of highly similar protein
646 pairs in testing and training, and the accuracy of RAPPID was largely stable with a small
647 improvement when highly similar testing proteins were excluded.

648

649 Developing appropriate and meaningful benchmark datasets for PPI prediction remains a
650 challenging problem for a number of reasons. Firstly, deep learning tasks rely on large, high-
651 quality datasets to obtain meaningful generalised models. Such datasets are few and far between.
652 Projects like HIPPIE and iRefWeb join STRING in being among the best examples of PPI
653 datasets which integrate multiple sources to assure both quality and quantity of PPI edges
654 (Alanis-Lobato *et al.*, 2017; Turner *et al.*, 2010). Despite this, STRING is the only dataset among
655 these three which has an appropriate number of high-confidence edges for the purpose of
656 learning deep learning model. Specifically, there are 98.5% fewer edges in HIPPIE than in
657 STRING between human proteins at a 95% confidence threshold. Even when confidence
658 thresholds are lowered to 85%, HIPPIE holds 87.9% fewer human edges than STRING.
659 Similarly STRING at a 95% confidence threshold has 75% more human edges when considering
660 iRefWeb edges with 3 supporting references or more.

661

662 Secondly, this reliance on large, representative datasets is further exacerbated by the unique
663 overfitting challenges posed by the characteristics of PPI data, as explored in this work and in
664 (Park and Marcotte, 2012). While RAPPID mitigates the overfitting tendencies of PPI data
665 through regularisation, it also relies on large, representative training data to do so. In the
666 construction of our C3 datasets, it is necessary to discard edges which are not between proteins
667 of the same validation split. As a result, we observe a further decrease of up to 33.9% in the
668 number of the already-precious-few edges afforded to us by STRING.

669

670 As we've shown in this work, the construction of benchmark datasets is critical for effectively
671 comparing and evaluating PPI prediction tasks. It is thanks to large, quality PPI dataset projects

672 like STRING that we might construct meaningful and appropriate datasets against which to
673 evaluate PPI prediction methods like RAPPID. Additional efforts and methodologies to collect
674 and integrate PPI edges of the scale of STRING at high confidence levels are greatly desired, as
675 they can help identify and mitigate biases that inevitably arise when constructing datasets.

676

677 The task of PPI prediction is related to the problem of protein docking inference, whereby
678 computational models predict the atomic interactions between two proteins. While many
679 methods have historically been based on the fast Fourier transform for energy evaluation (Desta
680 *et al.*, 2020), new and effective deep learning methods have also become available. One such
681 method is AlphaFold-multimer (Evans *et al.*, 2021), which builds upon a Transformer model for
682 the prediction of protein structure (Jumper *et al.*, 2021) to infer the interface of homo and hetero
683 protein dimers at an atomic level. Integrating docking predictions can be an interesting future
684 direction to help improve RAPPID's PPI prediction generalisation.

685

686 RAPPID's ability to predict interactions warrants further study into relevant tasks that might
687 benefit from a similar approach. The RAPPID architecture might be modified for the tasks of
688 binding site and protein function prediction. These tasks are related to PPI prediction and as a
689 result are exposed to similar challenges to which RAPPID is well suited. However, in all these
690 cases, it is crucial to consider strict rules for cross-validation and data splitting to ensure data
691 leakage is avoided.

692

693

694

695 **Funding:**

696 This work was supported by Natural Sciences and Engineering Research Council of Canada
697 (NSERC) grant RGPIN-2019-04460 (AE), and by McGill Initiative in Computational Medicine
698 (MiCM) (AE). This research was enabled in part by support provided by Calcul Québec
699 (www.calculquebec.ca) and Compute Canada (www.computeCanada.ca).

700

701

702 **Authors' contributions:**

703 AE and JS conceived the study, designed the project and the algorithm, and wrote the
704 manuscript. JS implemented the pipeline and performed the statistical analyses of the results. All
705 authors read and approved the final manuscript.

706

707

708 **References**

709

710 Alanis-Lobato,G. *et al.* (2017) HIPPIE v2.0: enhancing meaningfulness and reliability of
711 protein–protein interaction networks. *Nucleic Acids Res*, **45**, D408–D414.

712 Altschul,S.F. *et al.* (1990) Basic local alignment search tool. *Journal of Molecular Biology*, **215**,
713 403–410.

714 Altschul,S.F. *et al.* (1997) Gapped BLAST and PSI-BLAST: a new generation of protein
715 database search programs. *Nucleic Acids Research*, **25**, 3389–3402.

716 Anfinsen,C.B. (1973) Principles that Govern the Folding of Protein Chains. *Science*, **181**, 223–
717 230.

718 Athiwaratkun,B. *et al.* (2019) There Are Many Consistent Explanations of Unlabeled Data: Why
719 You Should Average. In, *ICLR*.

720 Ben-Hur,A. and Noble,W.S. (2006) Choosing negative examples for the prediction of protein-
721 protein interactions. *BMC Bioinformatics*, **7**, S2–S2.

722 Ben-Hur,A. and Noble,W.S. (2005) Kernel methods for predicting protein–protein interactions.
723 *Bioinformatics*, **21**, i38–i46.

724 Berman,H.M. (2000) The Protein Data Bank. *Nucleic Acids Research*, **28**, 235–242.

- 725 Blohm,P. *et al.* (2014) Negatome 2.0: a database of non-interacting proteins derived by literature
726 mining, manual annotation and protein structure analysis. *Nucl. Acids Res.*, **42**, D396–
727 D400.
- 728 Boekhout,A.H. *et al.* (2011) Trastuzumab. *Oncologist*, **16**, 800–810.
- 729 Brock,A. *et al.* (2021) High-Performance Large-Scale Image Recognition Without
730 Normalization. *arXiv:2102.06171 [cs, stat]*.
- 731 Bromley,J. *et al.* (1993) Signature verification using a “siamese” time delay neural network. *Int.*
732 *J. Patt. Recogn. Artif. Intell.*, **07**, 669–688.
- 733 Browne,F. *et al.* (2007) Supervised Statistical and Machine Learning Approaches to Inferring
734 Pairwise and Module-Based Protein Interaction Networks. In, *2007 IEEE 7th*
735 *International Symposium on BioInformatics and BioEngineering*. IEEE, Boston, MA,
736 USA, pp. 1365–1369.
- 737 Carpenter,E.P. *et al.* (2008) Overcoming the challenges of membrane protein crystallography.
738 *Current Opinion in Structural Biology*, **18**, 581–586.
- 739 Chen,H.H. *et al.* (2012) Novel Protein Therapeutics for Systolic Heart Failure: Chronic
740 Subcutaneous B-Type Natriuretic Peptide. *Journal of the American College of*
741 *Cardiology*, **60**, 2305–2312.
- 742 Chen,M. *et al.* (2019) Multifaceted protein–protein interaction prediction based on Siamese
743 residual RCNN. *Bioinformatics*, **35**, i305–i314.
- 744 Cong,Q. *et al.* (2019) Protein interaction networks revealed by proteome coevolution. *Science*,
745 **365**, 185–189.
- 746 Desta,I.T. *et al.* (2020) Performance and Its Limits in Rigid Body Protein-Protein Docking.
747 *Structure*, **28**, 1071-1081.e3.
- 748 Devlin,J. *et al.* (2019) BERT: Pre-training of Deep Bidirectional Transformers for Language
749 Understanding. *arXiv:1810.04805 [cs]*.
- 750 Dick,K. *et al.* (2020) PIPE4: Fast PPI Predictor for Comprehensive Inter- and Cross-Species
751 Interactomes. *Scientific Reports*, **10**, 1390.
- 752 Ding,Y. *et al.* (2016) Predicting protein–protein interactions via multivariate mutual information
753 of protein sequences. *BMC Bioinformatics*, **17**, 398.
- 754 Elnaggar,A. *et al.* (2021) ProtTrans: Towards Cracking the Language of Life’s Code Through
755 Self-Supervised Learning.
- 756 Evans,R. *et al.* (2021) Protein complex prediction with AlphaFold-Multimer Bioinformatics.
- 757 Falcon,W. *et al.* (2020) PyTorchLightning/pytorch-lightning: 0.7.6 release Zenodo.
- 758 Gillis,J. *et al.* (2014) Bias tradeoffs in the creation and analysis of protein–protein interaction
759 networks. *Journal of Proteomics*, **100**, 44–54.
- 760 Henikoff,S. and Henikoff,J.G. (1992) Amino acid substitution matrices from protein blocks.
761 *Proceedings of the National Academy of Sciences*, **89**, 10915–10919.
- 762 Hochreiter,S. (1998) The Vanishing Gradient Problem During Learning Recurrent Neural Nets
763 and Problem Solutions. *Int. J. Unc. Fuzz. Knowl. Based Syst.*, **06**, 107–116.
- 764 Hochreiter,S. and Schmidhuber,J. (1997) Long Short-Term Memory. *Neural Computation*, **9**,
765 1735–1780.
- 766 Huttlin,E.L. *et al.* (2017) Architecture of the human interactome defines protein communities and
767 disease networks. *Nature*, **545**, 505–509.

- 768 Izmailov,P. *et al.* (2019) Averaging Weights Leads to Wider Optima and Better Generalization.
769 *arXiv:1803.05407 [cs, stat]*.
- 770 Jansen,R. (2003) A Bayesian Networks Approach for Predicting Protein-Protein Interactions
771 from Genomic Data. *Science*, **302**, 449–453.
- 772 Jassal,B. *et al.* (2019) The reactome pathway knowledgebase. *Nucleic Acids Research*, gkz1031.
- 773 Jumper,J. *et al.* (2021) Highly accurate protein structure prediction with AlphaFold. *Nature*, **596**,
774 583–589.
- 775 Kanehisa,M. (2000) KEGG: Kyoto Encyclopedia of Genes and Genomes. *Nucleic Acids*
776 *Research*, **28**, 27–30.
- 777 Kudo,T. (2018) Subword Regularization: Improving Neural Network Translation Models with
778 Multiple Subword Candidates. *arXiv:1804.10959 [cs]*.
- 779 Kudo,T. and Richardson,J. (2018) SentencePiece: A simple and language independent subword
780 tokenizer and detokenizer for Neural Text Processing. In, *Proceedings of the 2018*
781 *Conference on Empirical Methods in Natural Language Processing: System*
782 *Demonstrations*. Association for Computational Linguistics, Brussels, Belgium, pp. 66–
783 71.
- 784 Li,Y. and Ilie,L. (2017) SPRINT: ultrafast protein-protein interaction prediction of the entire
785 human interactome. *BMC Bioinformatics*, **18**, 485.
- 786 Lipton,Z.C. *et al.* (2015) A Critical Review of Recurrent Neural Networks for Sequence
787 Learning. *arXiv:1506.00019 [cs]*.
- 788 Loshchilov,I. and Hutter,F. (2019) Decoupled Weight Decay Regularization. In, *ICLR*.
- 789 Malenfant,S.J. *et al.* (2014) Pertuzumab: a new targeted therapy for HER2-positive metastatic
790 breast cancer. *Pharmacotherapy*, **34**, 60–71.
- 791 Merity,S. *et al.* (2017) Regularizing and Optimizing LSTM Language Models.
792 *arXiv:1708.02182 [cs]*.
- 793 Misra,D. (2020) Mish: A Self Regularized Non-Monotonic Activation Function.
794 *arXiv:1908.08681 [cs, stat]*.
- 795 Orchard,S. *et al.* (2012) Protein interaction data curation: the International Molecular Exchange
796 (IMEx) consortium. *Nature Methods*, **9**, 345–350.
- 797 Orchard,S. *et al.* (2014) The MIntAct project—IntAct as a common curation platform for 11
798 molecular interaction databases. *Nucl. Acids Res.*, **42**, D358–D363.
- 799 Oughtred,R. *et al.* (2020) The BioGRID database: A comprehensive biomedical resource of
800 curated protein, genetic, and chemical interactions. *Protein Science: A Publication of the*
801 *Protein Society*, **30**, 187–200.
- 802 Park,Y. and Marcotte,E.M. (2012) Flaws in evaluation schemes for pair-input computational
803 predictions. *Nat Methods*, **9**, 1134–1136.
- 804 Paszke,A. *et al.* (2019) PyTorch: An Imperative Style, High-Performance Deep Learning
805 Library. In, Wallach,H. *et al.* (eds), *Advances in Neural Information Processing Systems*
806 **32**. Curran Associates, Inc., pp. 8024–8035.
- 807 Richoux,F. *et al.* (2019) Comparing two deep learning sequence-based models for protein-
808 protein interaction prediction. *arXiv:1901.06268 [cs, q-bio, stat]*.
- 809 Roux,K.J. *et al.* (2012) A promiscuous biotin ligase fusion protein identifies proximal and
810 interacting proteins in mammalian cells. *Journal of Cell Biology*, **196**, 801–810.

- 811 Salwinski,L. *et al.* (2004) The Database of Interacting Proteins: 2004 update. *Nucleic Acids Res.*,
812 **32**, D449-451.
- 813 Schuster,M. and Nakajima,K. (2012) Japanese and Korean voice search. In, *2012 IEEE*
814 *International Conference on Acoustics, Speech and Signal Processing (ICASSP)*., pp.
815 5149–5152.
- 816 Sikder,S. *et al.* (2019) Long-term delivery of protein and peptide therapeutics for cancer
817 therapies. *Expert opinion on drug delivery*.
- 818 Snider,J. *et al.* (2015) Fundamentals of protein interaction network mapping. *Mol Syst Biol*, **11**,
819 848.
- 820 Srivastava,N. *et al.* (2014) Dropout: a simple way to prevent neural networks from overfitting. *J.*
821 *Mach. Learn. Res.*, **15**, 1929–1958.
- 822 Szklarczyk,D. *et al.* (2019) STRING v11: protein–protein association networks with increased
823 coverage, supporting functional discovery in genome-wide experimental datasets. *Nucleic*
824 *Acids Res*, **47**, D607–D613.
- 825 Tabe-Bordbar,S. *et al.* (2018) A closer look at cross-validation for assessing the accuracy of gene
826 regulatory networks and models. *Sci Rep*, **8**, 6620.
- 827 Tsomaia,N. (2015) Peptide therapeutics: targeting the undruggable space. *European journal of*
828 *medicinal chemistry*.
- 829 Turner,B. *et al.* (2010) iRefWeb: interactive analysis of consolidated protein interaction data and
830 their supporting evidence. *Database*, **2010**, baq023–baq023.
- 831 Usmani,S. *et al.* (2017) THPdb: Database of FDA-approved peptide and protein therapeutics.
832 *PloS one*.
- 833 Vaswani,A. *et al.* (2017) Attention is all you need. In, *Proceedings of the 31st International*
834 *Conference on Neural Information Processing Systems, NIPS’17*. Curran Associates Inc.,
835 Red Hook, NY, USA, pp. 6000–6010.
- 836 Vidal,M. and Fields,S. (2014) The yeast two-hybrid assay: still finding connections after 25
837 years. *Nat Methods*, **11**, 1203–1206.
- 838 Wan,L. *et al.* (2013) Regularization of Neural Networks using DropConnect. In, Dasgupta,S. and
839 McAllester,D. (eds), *Proceedings of the 30th International Conference on Machine*
840 *Learning*, Proceedings of Machine Learning Research. PMLR, Atlanta, Georgia, USA,
841 pp. 1058–1066.
- 842 Wright,L. and Demeure,N. (2021) Ranger21: a synergistic deep learning optimizer.
843 *arXiv:2106.13731 [cs]*.
- 844 Yang,J. *et al.* (2012) BioLiP: a semi-manually curated database for biologically relevant ligand–
845 protein interactions. *Nucleic Acids Research*, **41**, D1096–D1103.
- 846 Yong,H. *et al.* (2020) Gradient Centralization: A New Optimization Technique for Deep Neural
847 Networks. In, *ECCV*.
- 848 Yosinski,J. *et al.* (2014) How transferable are features in deep neural networks? In,
849 Ghahramani,Z. *et al.* (eds), *Advances in Neural Information Processing Systems 27*.
850 Curran Associates, Inc., pp. 3320–3328.
- 851 Zaremba,W. *et al.* (2015) Recurrent Neural Network Regularization. *arXiv:1409.2329 [cs]*.
- 852 Zhang,M.R. *et al.* (2019) Lookahead Optimizer: k steps forward, 1 step back. In, *NeurIPS*.